Fabrication and characterization of 15Cr-15Ni austenitic steel cladding tubes for sodium fast reactors

E. Curtet, Patrick Olier, Émilien Curtet, Stéphane Urvoy, Matthew Bono, Arnaud Courcelle

ICAPP 2019 – International Congress on Advances in Nuclear Power Plants
France, Juan-les-pins – 2019, May 12 │15

000108 - Fabrication and characterization of 15Cr-15Ni austenitic steel cladding tubes for sodium fast reactors

Patrick Olier [1*], Emilien Curtet [1], Stéphane. Urvoy [1], Matthew Bono [2], Arnaud Courcelle [2]

1. DEN-Service de Recherches Métallurgiques Appliquées, CEA, Université Paris-Saclay, F-91191, Gif-sur-Yvette, France
2. DEN-Service d'Etudes des Matériaux Irradiés, CEA, Université Paris-Saclay, F-91191, Gif-sur-Yvette, France

* Corresponding author: patrick.olier@cea.fr

Abstract - Two fabrication routes requiring industrial facilities are being conducted to produce several hundred 15Cr-15Ni cladding tubes. The processing methods involve varying degrees of cold work and different heat treatment conditions. In order to ensure that the specifications are fulfilled, both batches of tubes are fully characterized regarding several aspects. The microstructure is observed using optical and electron microscopy. A refinement of the grain size is detected in the inner diameter of one batch, which is caused by a nitrogen contamination revealed by glow discharge mass spectrometry analysis. The precipitates are also carefully analyzed. Selective dissolutions are performed on both batches to determine their mass fractions. The precipitates (TiC, TiN and Ti_2CS) are identified using X-ray diffraction. The titanium content in solid solution is measured and the resulting values are analyzed to assess the quality of the last solution annealing. The tensile properties measured at room temperature comply with those expected for this steel grade. On the basis of our results and considering past experience with cladding irradiated in Phenix reactor a good behavior in pile can be foreseen for these tubes.

KEYWORDS: 15Cr15Ni-Ti austenitic steels, sodium fast reactor, cladding tubes, fabrication

Introduction

The world's first sodium fast reactors (SFR) were put in service in the 1950s, and the current fleet is comprised of thirteen units. Of these thirteen, eight are research reactors and six are power reactors. Among the power reactors four are currently in service: BOR-60 and BN-600 in Russia, CEFR (China Experimental Fast Reactor), and FBTR (Fast Breeder Test Reactor) in India. It should be noted that advanced austenitic steels were selected in all cases for the cladding material of the fuel assembly. These steels grade exhibit good formability and weldability, compatibility with sodium, corrosion resistance, and suitable mechanical properties at the service temperature (400-700°C). Above all, there are not susceptible to excessive swelling under irradiation, even for significant doses until 100 dpa, which would allow very high burn-up fractions to be reached for the core (> 150 GWd/t_{ML}). Different austenitic steel grades are used in each country:

- In Russian reactors, such as BN-600, damage doses up to 90 dpa are achieved with ChS-68 cold-worked (16Cr15NiMoNbMnTi) steel, and a program for achieving damage doses of 120-140 dpa for this grade has been designed [1].
- The grades 3Chs-68 and 316Ti are used for CEFR cladding, while the "CN-1515(Ti)" is preferred for CFR 600 (China Fast Reactor) which is under construction on the Xiapu site [2].
- The D9 (15Cr-15Ni-0,2Ti) alloy was selected for the Indian FBTR, and an optimization of the composition is being studied for the future PFBR (Prototype Fast Breeder Reactor) [3].
- The Japanese-prime-candidate-alloy (JPCA) is also a Ti-stabilized austenitic steel [4] selected for SFR systems such as Monju and Joyo. Concerning Monju, a decommissioning plan was approved by Japan Regulator in 2017 while Joyo is currently being repaired.
- In addition, cold worked austenitic DIN 1.4970 (15-15Ti) is the selected candidate for the concept reactor ADS MYRRHA, which will be cooled by lead-bismuth [5,6].

In France, the experience acquired over the thirty-six years of operation of Phenix and the construction and the operation of two cores of Superphenix, as well as the studies associated with the EFR (European Fast Reactor) program, yielded a great deal of knowledge available for the GEN IV SFR program. In the prospect of deploying sodium cooled fast reactors, the CEA proposed a Simulation Program for SFRs at the end of 2017. It includes some R&D studies on core materials in the continuity of those undertaken for the ASTRID project [7,8,9].

Titanium-stabilized austenitic steels have been selected as the reference material for fuel pin cladding. By improving the chemical composition and the degree of cold work, damage doses of up to 100 dpa can be sustained by the French 15Cr-15Ni steel, the so called AIM1 (Austenitic Improved Material #1).
In the scope of the ASTRID project, two fabrication routes requiring industrial facilities (cold pilgering and drawing benches, and continuous mill annealing furnaces) are being used to produce an amount of three hundred 15Cr15Ni-Ti cladding tubes. The processing methods involve varying degrees of cold work and different heat treatment conditions. In particular, different temperatures and durations of the final solution annealing step are used by the manufacturers, which should have an effect on the precipitate fraction and the grain size.
In order to ensure that the specifications are fulfilled, both batches of tubes are fully characterized regarding several features (grain size, precipitates, and tensile properties). The results reveal some differences between the two batches of tubes, which are analyzed in relation to the fabrication methods.

Specific requirements and manufacturing routes

The specifications for the fabrication of the cladding tubes are based on experience gained from the production of similar tubes for the Phenix reactor. These specifications concern the ingot, the semi-finished products, and the finished tubes.
In addition to the analysis of the steel composition and the measurement of the fraction of inclusions performed on the ingot, the grain sizes and the mechanical properties must be checked on the tubes after the last solution anneal and after the last drawing pass. Furthermore, the chemical composition, the cleanliness and the surface roughness are inspected on the finished tubes. Metrological instruments and non-destructive facilities (ultrasonic and eddy current testing) are used to measure the final dimensions with respect to the required tolerances (diameters, circularity, and straightness) and the absence of defects.
On this basis, a heat of about six tons of AIM1 was melted by Aubert & Duval using induction melting followed by vacuum arc remelting [7]. Primary shapes obtained by hot forging were used to manufacture two batches of cladding tubes using the fabrication schemes shown in figures 1 and 2.
- The first batch was obtained by hot extrusion of a hollow shape, followed by cold pilgering and several passes of cold drawing, interrupted by intermediate annealing.
- The second batch was obtained by double extrusion of a bar, followed by a drilling operation and a cold drawing sequence, with intermediate annealing.
A few hundred were fabricated. For the batch PB1, the tubes were solution annealed (SA) at 1105°C for 30 seconds, followed by a cold drawing of 23% cold work. For the batch ST1, the tubes were solution annealed at 1130°C for 3 minutes and 30 seconds, followed by 20% cold work. The tubes were characterized in the as-received condition.

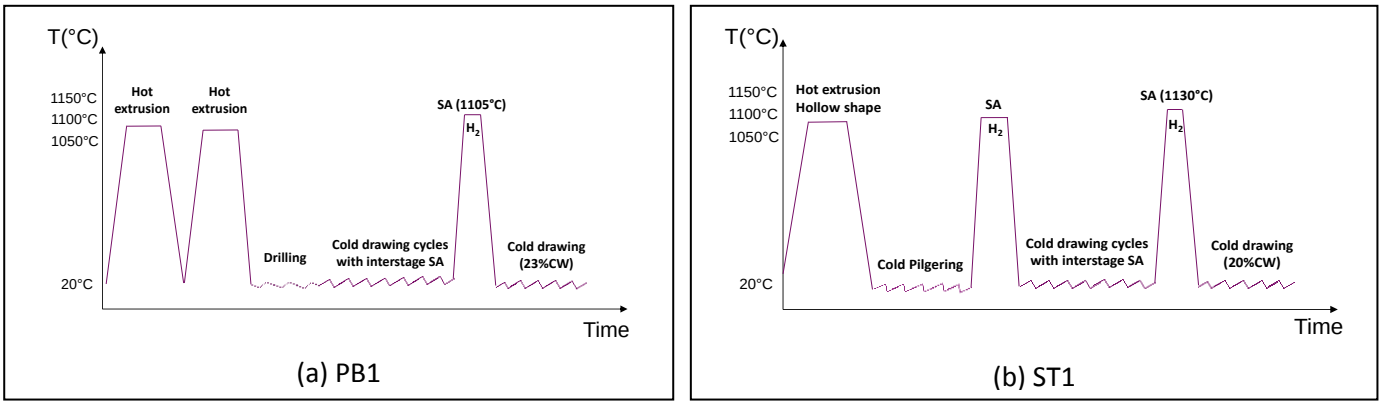

Figure 1 : Diagram of fabrication process a) for PB1 and b) for ST1

The chemical composition was measured by the supplier of the ingot using Optical Emission Spectroscopy (OES), Plasma Emission Spectrometry (PES), Combustion and Infrared Absorption (CIA) or Thermal Conductibility (TC). The main alloying elements and the analysis method used are reported in Table 1.

Table 1: Main alloying elements of 1515-Ti AIM1 (in weight percent)

	Cr	Ni	C	Mo	Mn	Si	Ti	P	N	S
Weight%	14.3	15.0	0.091	1.52	1.42	0.84	0.40	0.046	0.006	0.0009
Uncertainty	±0.7	±0.7	±0.001	±0.12	±0.09	±0.05	±0.01	±0.006	±0.001	±0.003
Method	*OES*	*PES*	*CIA*	*OES*	*OES*	*OES*	*OES*	*OES*	*TC*	*CIA*

Microstructural analysis

Optical microscopy and chemical analysis

Figure 2 shows the optical micrographs obtained for both batches. The microstructure exhibits equiaxed grains in the cross sections, while the grains are slightly elongated in the longitudinal direction parallel to the drawing direction. The grain aspect ratio (i.e. length in the longer direction / length in the shorter direction) is estimated at 1.4 and 1.8, respectively for ST1 and PB1 (based on the measurement of 250 grains by image analysis for each sample). The grain size measured in the transverse direction is similar for both batches with a G value of 8 according to the NF EN ISO 643 (corresponding to a mean diameter of 22 µm). A few coarser grains of up to 50 µm in size (encircled in green) are evident in the micrographs.

Interestingly, the higher degree of cold work coupled with a lower SA temperature used for PB1 did not result in a refinement of the grain size. This result could possibly be linked to the different manufacturing methods used for the batchs of tubes prior to the final SA. Note that SP1 was subjected to a greater degree of cold work processing by cold pilgering and subsequent cold drawing compared to PB1, which had only one cold drawing stage after two operations of hot extrusion to reach a diameter of 40 mm.

Typical coarse primary orange-coloured precipitates of a size of a few micrometers are evident in figure 2c-2d. Sometimes identified as titanium nitrides, EDS maps reveal that they also contain carbon and molybdenum. Smaller carbides of a few hundred nanometers (usually identified as (Ti,Mo)C in this grade of steel) can also be seen. Some of them are aligned in the drawing direction.

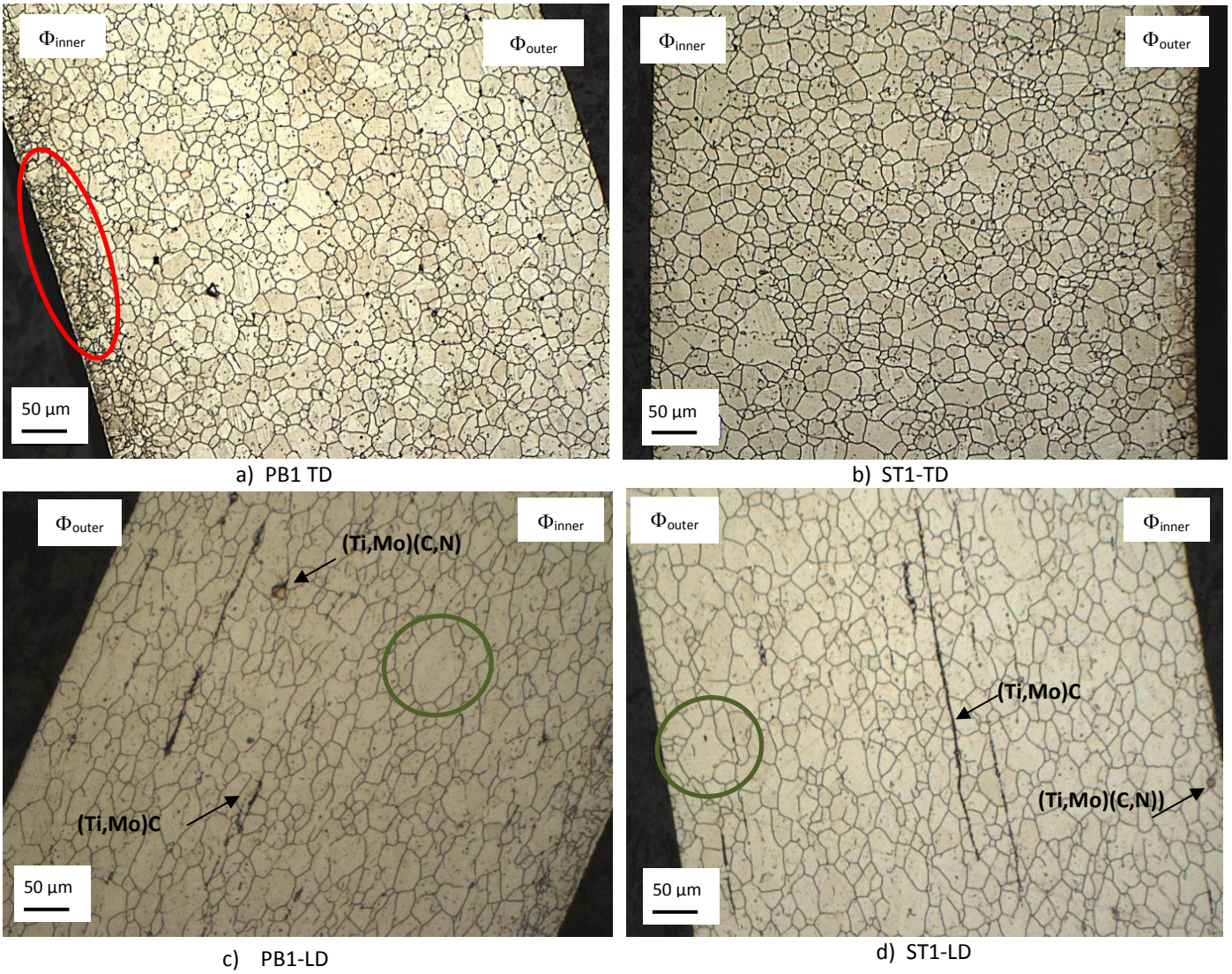

Figure 2 : Optical micrographs for PB1 and ST1 in the transverse and longitudinal directions (TD and LD)

The micrographs for PB1 reveal a fine grain layer on the inner diameter (G value ranging from 10 to 11, i.e. a mean diameter between 7 and 11 µm). It was verified that this zone with very fine grains (encircled in red in figure 2a) is present over the entire length of the tube.

Some thickness of this fine layer was measured using the « Videomet » software (see Figure 3). The mean value obtained is about 30 µm (Table 2).

Table 2: Thickness of the fine grain layer measured at the inner diameter on transverse and longitudinal sections – PB1)

Zone of the tube	Average Thickness (µm)		Standard deviation
	Transverse	Longitudinal	
End of the tube	30.6	32.6	2.4
Middle of the tube	27.6	29.2	2.3

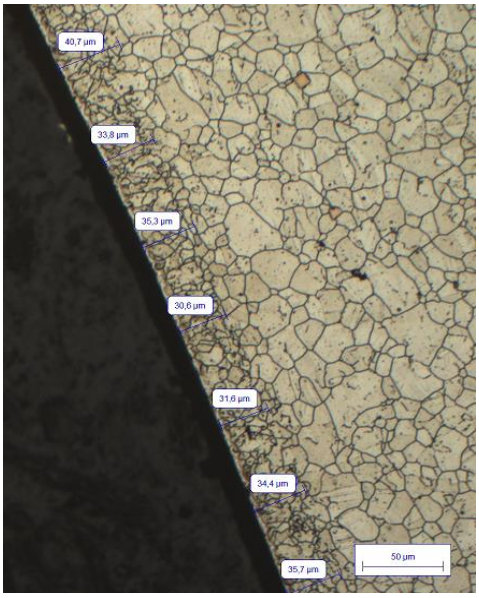

Figure 3 : Measurement of the thickness of the fine grain layer (PB1 sample)

As a decrease of the grain size can lead to an increase of the hardness, according to the Hall-Petch law, microhardness profiles were performed under a load of 50 g with a Leica VMHT 30A device. For each tube, 20 indentations were measured, however there was no significant difference in hardness between the inner and outer diameters. The hv50 average values are about 335 ± 21 and 336 ± 20 Vickers at the inner diameter side and at the outer diameter side respectively. So, the absence of Hall-Petch effect remains a point to clarify.
Knowing that nitrogen is an element that can lead to grain size refinement [10], analyses by Glow Discharge Mass Spectrometry (GDMS) were carried out with a Horiba Scientific device (model Profiler 2) to determine the nitrogen profiles on the inner and outer surfaces of the tubes. The analysis equipment consists of a source with luminescent discharge coupled with an optical spectrometer and an ultrafast data acquisition system.
The nitrogen content in the samples is close to the limit of detection (100 to 150 ppm), so the raw values obtained by this analysis should be considered with caution. However, it is possible to compare the trends between both samples. Figure 4 presents the nitrogen profiles for the inner and outer surfaces of tubes ST1 and PB1.

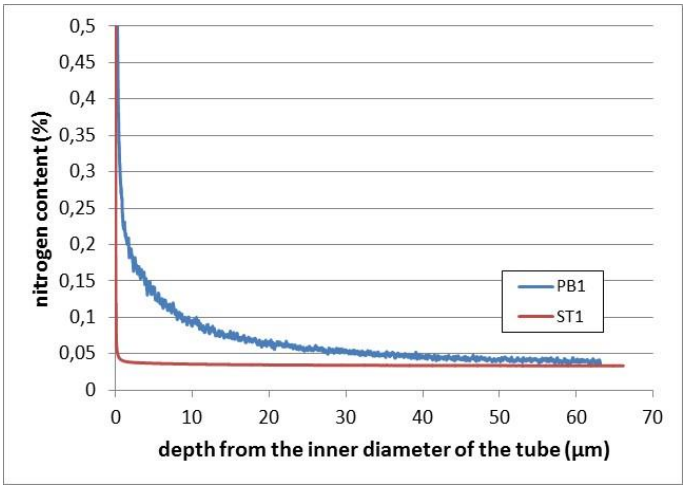

(a)

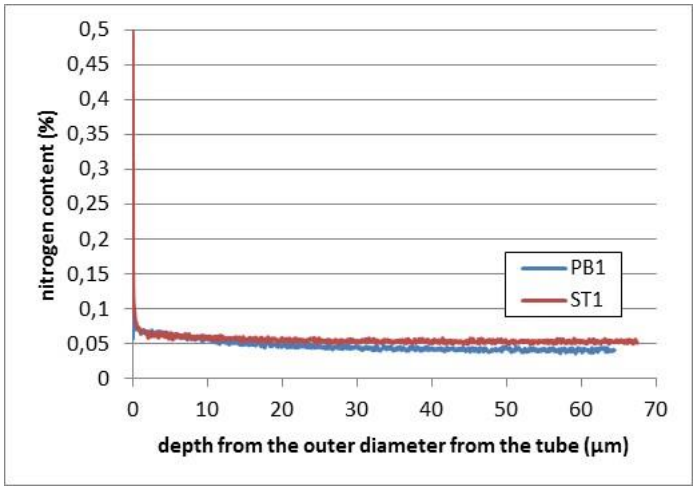

(b)

Figure 4: Nitrogen profiles obtained from the inner (a) and outer (b) diameters for PB1 and ST1 respectively

For PB1, the nitrogen surface analysis performed starting from the inner diameter shows a gradual decrease from about 0.3% at the surface to 0.04% at a depth of about 50 µm. The nitrogen profile seems to remain constant thereafter. For ST1, the nitrogen profile remains at about 0.04% after a depth of only a few micrometers from the inner surface of the tube. On the outer surface of both batches, the nitrogen content is close to 0.05% regardless of depth.
The nitrogen surface analyses have revealed a nitrogen contamination on the inner diameter side of batch PB1. This contamination leads to a grain refinement over a depth of a few tens of micrometers, as evidenced by the metallographic examinations. Note that no carbon contamination was revealed by performing the same kind of analysis.

The nitrogen contamination probably comes from the presence of air trapped inside the tubes during heat treatments in the continuous mill annealing furnaces. Although heat treatments are performed under gaseous protection from hydrogen, it is well known that the gas convection can be disrupted for long tubes. To avoid such problems, many manufacturers do a systematic air bleeding before introducing the tubes in the furnace. This type of bleeding process was not performed by the manufacturer of the PB1 tubes.

TEM examination

Microstructural analyses were performed on thin foil specimens with a 300 kV FEI TECNAI 30 G2 TEM (LaB6 filament) equipped with an ORIUS 200D GATAN CCD Camera.
Many grains are heavily twinned as shown in Figure 5a-5d. TEM examinations also reveal a high dislocation density due to the cold working. The dislocation network can be in the form local rearrangements into cells (see figure 5b-5e). The diameters of these dislocation cells can reach a few hundred nanometers. Only primary precipitates are present (for example three white (Ti,Mo)C precipitates are visible in figure 5b). No (Ti,Mo)C nanoprecipitates and no rich-Cr carbides were detected as expected for unaged and/or unirradiated conditions.
A few triangular-shaped defects were also observed with the sample oriented in the two beam condition B=[110] g=<002> as shown in figure 5c-5f. Triangular-shaped contrasts in TEM images can be the result of overlapping defects in the electron beam direction. Stacking Fault Tetrahedra (SFT) also have a similar contrast but have rarely been observed in such steels in the absence of irradiation [11,12]. Further examinations are needed to determine the nature of these defects.
It can be pointed out that no significant differences were detected between the two batches of tubes.

PB1

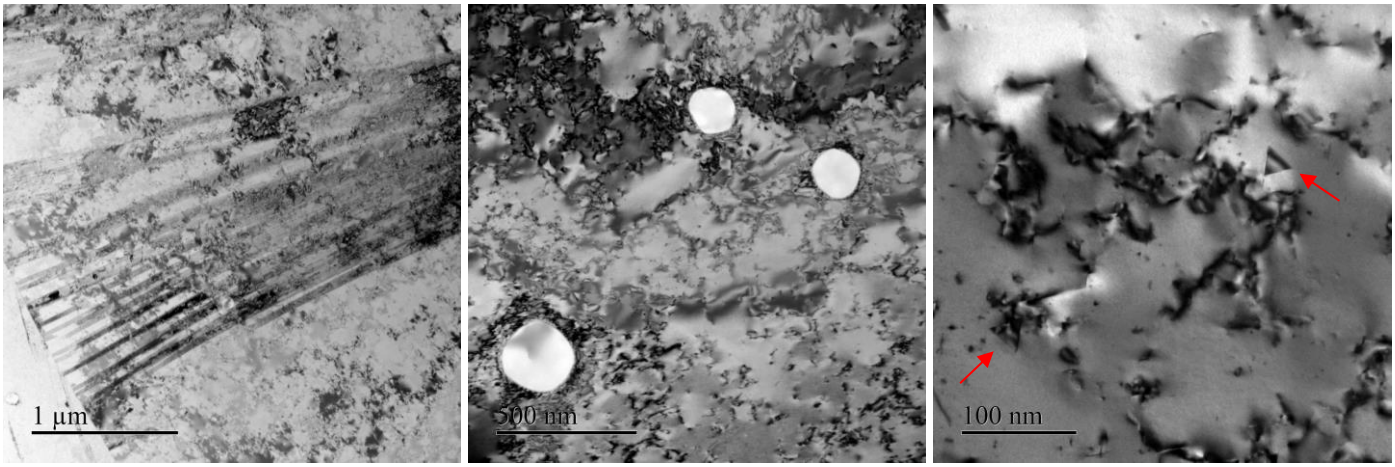

a) b) c)

ST1

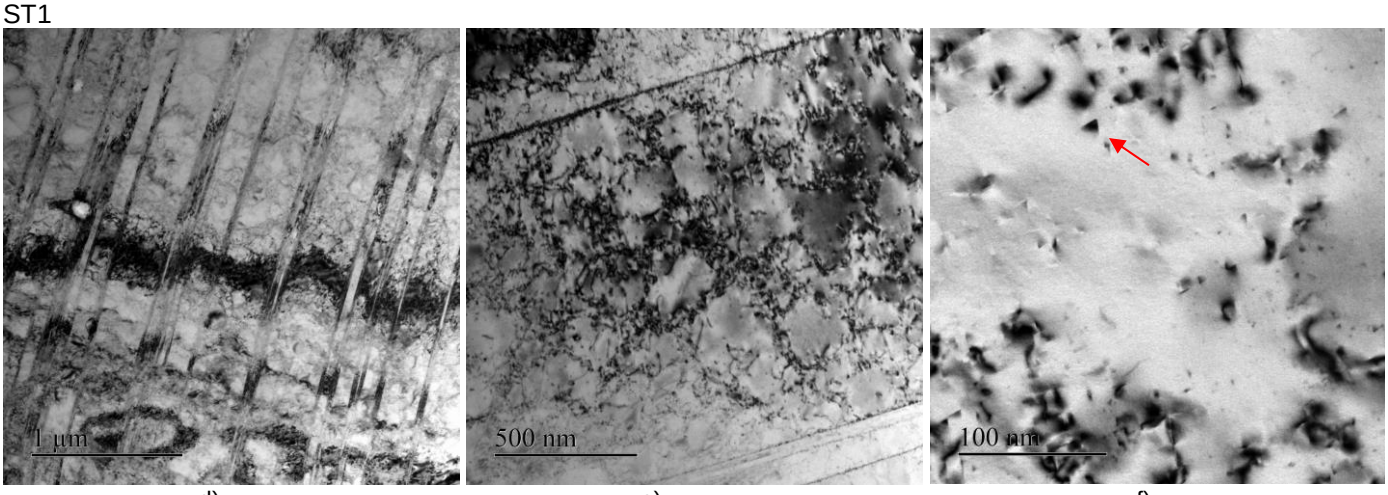

d) e) f)

Figure 5 : Bright-field TEM micrographs showing the general microstructure with twins, high dislocation density and few dislocation cells as well as TiMoC precipitates and triangular-shaped defects (right images) indicated by the red arrows

Analysis of the precipitates

The final solution annealing step is intended to dissolve the primary titanium carbides into solid solution. In this manner, the titanium atoms are free to form nanometric carbides that pin the dislocation network and stabilize it at the service temperature of the reactor. The stabilized dislocation network then acts as a sink for irradiation defects, thereby reducing the irradiation swelling of the fuel cladding during reactor service [13]. In order to determine the

efficiency of the solution annealing step, the material was dissolved in acid, and the precipitates were filtered out of the liquid solution. The filter collects only precipitates that are larger than its pore size, which in this case was approximately 220 nm. By measuring the mass of the collected primary titanium carbides and comparing it to the mass of metal dissolved, the effectiveness of the solution annealing process can be determined.
The weight ratio of precipitate is measured by using selective electrochemical dissolution of the alloy matrix using the method described in [14]. The experimental procedure requires the use of three 100 mm long specimens in order to dissolve about 24 grams of metal for each batch of tubes (see figure 6).

Figure 6 : Photographs of a sample before and after selective dissolution and the collected residue on a nitrocellulose filter with a pore size of 220 nanometers

Two selective dissolutions were performed leading to a precision of 0.02% on the measured fraction of precipitates In addition, the filtered solutions coming from selective dissolutions (which contain, in addition to the solvent, the matrix of the dissolved AIM1) were analyzed using a spectrometer with inductive coupling (ICP) connected to an optical spectrometer. The device used (OPTIMA 8300 DV of Perkin Elmer) indicates the concentration of the elements of interest in the liquid solution (Fe, Cr, Ni, Mn, Mo, Si and Ti).
The titanium mass fraction in the filtrate is calculated by dividing the titanium content by the sum of all metallic elements present in the filtrate. Thus, it is possible to deduce the titanium content in the matrix compared to the nominal titanium content in the alloy (0.40% in weight for the both batches). The results are reported in Table 3.

Table 3: Mass fraction of precipitates and chemical analysis of the filtrate

	PB1 (1105°C)			ST1 (1130°C)		
Mass fraction of precipitate (wgt %) *	0.34 – 0,35			0.30 – 0,30		
Chemical analysis of the metallic element in the filtrate coming from the selective dissolution (mg/l)*	Fe 3950	Cr 870	Ni 805	Fe 3632	Cr 805	Ni 838
	Mn 78	Mo 76	Si 25	Mn 72	Mo 69	Si 21
	Ti 10.5			Ti 8.8		
Titanium mass fraction in the filtrate (wgt %)	0.16			0.18		
C_{Ti} (solid solution) / C_{Ti} (ingot) (%)	40			45		

**average values obtained from the ICP-MS analysis of 2 x3 samples for each residue*

The total mass fraction of precipitates measured is reproducible for the same solution annealing with a percentage of about 0.34% and 0.30 % for PB1 and ST1 respectively. For ST1, the lower mass fraction value can be explained by the higher temperature used for the last solution annealing step (1130°C instead of 1105°C) which is consistent with the more efficient titanium dissolution.
The titanium fraction in solid solution is inversely proportional to the mass fraction of precipitate. At 1130°C, the percentage is 45%, and at a lower temperature (1105°C) this fraction is only around 40%. It is correlated with the fact that titanium is the main element present in the precipitates (TiC) or (Ti,Mo)C primary/secondary carbides) as revealed by X-ray diffraction analysis (see below in Figure 7).
By referring to results obtained on cladding irradiated in Phenix [13], which was composed of an AIM1-precursor steel, a good swelling resistance in pile can be expected if the total mass fraction of primary precipitates is below 0.45% and if the titanium fraction in solid solution is at least 45%. On the basis of our results, it appears that the titanium fraction in solid solution is slightly low for PB1, probably due to the relatively low SA temperature (1105°C) coupled with the short holding time (30 seconds).

To investigate the phase content of the collected residue, X-ray diffraction (XRD) investigations were performed using a Bruker D8-advance diffractometer using the Bragg-Brentano parafocusing geometry and a q-q configuration. The EVA-Bruker software is used for indexing diffractograms. It is coupled to the ICDD PDF-4+ database.
The X-ray diffraction patterns are similar for both tubes (ST1 and PB1), indicating the same phases in each case. As an example, the X-ray diffraction pattern obtained for the ST1 tube is shown in Figure 7.

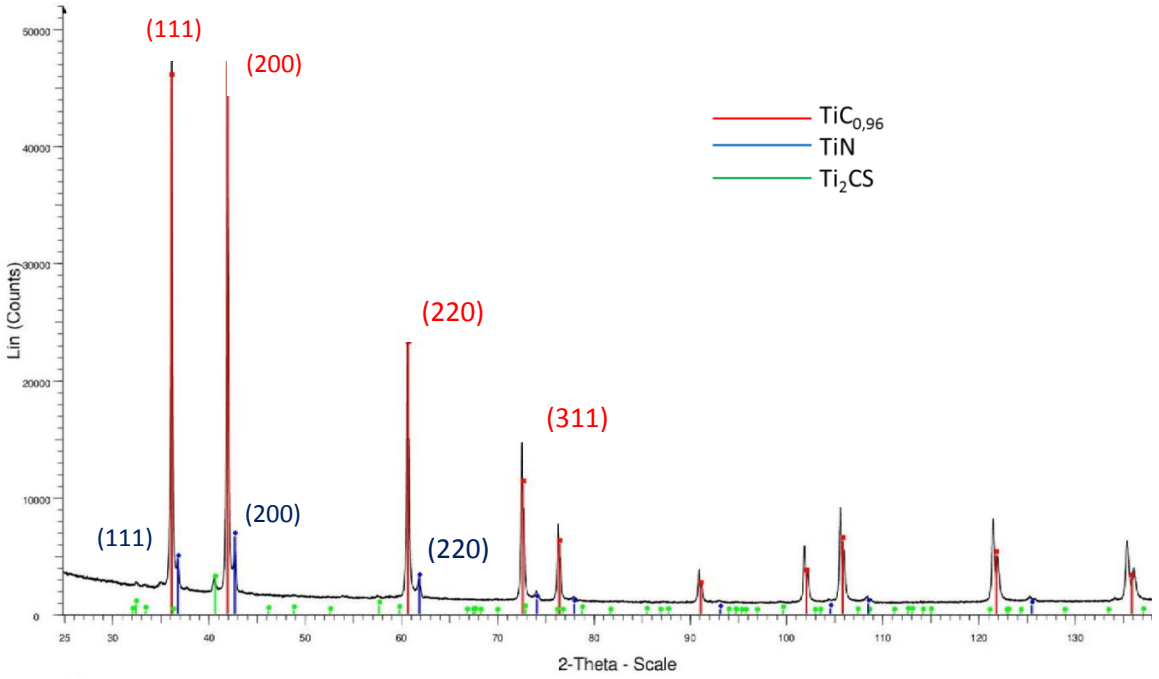

Figure 7 : X-Ray diffraction pattern for ST1

The current phases have been identified by comparing with the databases: it consists predominantly of titanium carbides ($TiC_{0,96}$) and titanium nitrides (TiN) with a face-centered cubic structure (FCC) and carbosulfides (Ti_2CS) with a hexagonal structure. The lattice parameters reported in table 4 are very close to the reference values coming from ICDD-PDF-4+ database. Note that our results are consistent with those obtained by other authors. It can be assumed that the titanium nitrides also contain some carbon and molydbdenum which is in agreement with X-Ray measurements performed by [15] and WDS X-ray map on AIM1 steel [14] respectively. The presence of molybdenum in titanium carbides ($TiC_{0,96}$) could not be verified on the basis of this indexation method, but many authors have detected it combining different analysis method such as EDX, WDS or electron energy loss spectroscopy [14,15,16,17,18].

Table 4: Lattice parameters obtained for ST1 and PB1 and results obtained by other authors

Phase	Reference Lattice parameters (ICDD-PDF-4+) (Å)	Our measurement (Å)	Other authors (Å)
$TiC_{0,96}$	$a_0 = 4.325$	$a_0 = 4.3256 \pm 1.10^{-4}$ (ST1) $a_0 = 4.3259 \pm 1.10^{-4}$ (PB1)	$a_0 = 4,288$ (Ti,Mo)C [17] $a_0 = 4,323$ (Ti,Mo)C [15]
TiN	$a_0 = 4.244$	$a_0 = 4.2493 \pm 1.10^{-4}$ (ST1) $a_0 = 4.2492 \pm 1.10^{-4}$ (PB1)	$a_0 = 4.242$ TiN with 9.6% C [18] $a_0 = 4.252$ Ti(N,C) [15]
Ti_2CS	a = 3.21 c = 11.2	$a = 3.208 \pm 1.10^{-3}$ (ST1) $c = 11.244 \pm 1.10^{-3}$ (ST1) $a = 3.209 \pm 1.10^{-3}$ (PB1) $c = 11.243 \pm 1.10^{-3}$ (PB1)	

Phase fractions were estimated by using two methods for each tube:
- 1) by comparing the intensity ratio of a plan family to a reference I/I_{cor} value determined in the ICDD data sheets (the (200) diffraction line was selected for $TiC_{0,96}$ and TiN while the (103) diffraction line was selected for Ti_2CS);
- 2) by full profile quantitative Rietveld refinement using the Fullprof software.

The results are reported in table 5.

Table 5: Phase fraction (in weight percent) obtained from XRD analysis

Phase	ST1		PB1	
	Method 1……	Method 2	Method 1……	Method 2
$TiC_{0,96}$	93.0 ± 1.3	91.9 ± 1.2	94.1 ± 1.4	93.4 ± 1.1
TiN	5.5 ± 0.4	5.9 ± 0.3	4.5 ± 0.6	5.1 ± 0.4
Ti_2CS	1.6 ± 0.3	2.2 ± 0.2	1.3 ± 0.5	1.5 ± 0.2

The results are quite close with both methods even if the uncertainty ranges for Ti_2CS do not overlap for ST1. It can be seen that for both samples, the proportion of TiC is heavily predominant (more than 90% in weight). It was also noted that the proportion of secondary carbides ($TiC_{0,96}$) in the ST1 tube is slightly lower than in the PB1 tube. At the same time, the mass fraction of primary carbides (TiN) is higher for the ST1 sample. Thus, the dissolution of the secondary carbides was more efficient for the ST1 sample, probably because of the higher SA temperature.

Results of tensile tests

The tensile properties were measured directly on tubes using a class 1 tensile testing machine according to EN ISO 6892-1. Three specimens were tested at room temperature (RT) for each batch, and an additional ST1 specimen was tested at 200°C. The speed rate was $3.3.10^{-6}$ m/s for determining the yield strength (YS) and $8.3.10^{-6}$ m/s for measuring the ultimate tensile strength (UTS) and the total elongation (TE).The results are reported in Table 6.

Table 6 : Tensile properties obtained for PB1 and ST1

Sample / Test Temperature / Jauge length	UTS (MPa)	YS (MPa)	TE (%)
PB1 / RT / l_0 = 25 mm	782 – 770 - 786	715 – 698 - 702	27.0 – 27.8 – 25.0
ST1 / RT / l_0 = 21 mm	766 – 767 - 775	683 – 677- 690	29.1 – 33.6 – 31.1
ST1 / 200°C / l_0 = 21 mm	680	623	12.8

The tensile properties obtained at RT are in accordance with those expected for this grade of steel [14]. A higher level of mechanical strength and a smaller total elongation were measured for PB1, in agreement with the higher degree of cold work (ε = 23% for PB1, as opposed to ε = 20% for ST1).
It can be pointed out that for ST1, the total elongation decreases drastically when the temperature increases from 20°C to 200°C. This singularity is due to a modification of the deformation mechanisms and the dislocation structure and is being studied at CEA [19]. However, it must be emphasized that the level of ductility returns to higher values for test temperatures corresponding to operating temperatures (400 - 700°C) of the cladding tubes [19]. Therefore, the measured TE can be considered good enough for reactor applications.

Conclusion

Two fabrication methods were conducted to produce a few hundred 15Cr15Ni-Ti cladding tubes in the scope of the ASTRID project. These tubes were characterized to make sure that they meet the specifications.
The microstructure was observed using optical and electron microscopy. A refinement of the grain size was detected at the inner diameter of one batch, which is caused by a nitrogen contamination that was detected by glow discharge mass spectrometry analysis.
The precipitates were also analyzed. Selective dissolutions were performed on both batches to determine the mass fractions of the primary precipitates. These precipitates (TiC, TiN and Ti_2CS) were identified using X-ray diffraction. The measured mass fractions of the precipitates are consistent with the expected values. In connection with that issue, the titanium content measured in solid solution represents respectively 40% and 45% (for PB1 and ST1) of the total amount of titanium in the alloy. The lower value obtained for PB1 probably is due to the lower SA temperature and the shorter holding time used for the last solution annealing.
The tensile properties measured at room temperature comply with those required [14].
On the basis of these results and considering past experience with cladding irradiated in Phenix a good behavior in pile can be foreseen for these tubes especially for ST1.

Aknowledgments

The authors wish to acknowledge EDF for financial support of this work. Thanks to Michel Tabarant from CEA/DPC/SEARS for his contribution to the chemical analyses of the tubes and the selective dissolution experiments, and to Justine Roubaud from CEA/DEN/SRMA for the XRD measurements.

References

[1] S.I. Porollo, Yu.V. Konobeev, F.A. Garner, Journal of Nuclear Materials 393 (2009) 61–66

[2] Donghui Zhang, “Nuclear Energy and Fast Reactor in China”, 49th Meeting Of The Technical Working Group On Fast Reactors, Buenos-Aires, May 2016

[3] Baldev Raj, Divakar Ramachandran and M. Vijayalakshmi, “OVERVIEW Development of cladding materials for sodium-cooled fast reactors in India”, Transactions of The Indian Institute of Metals Vol. 62, Issue 2, April 2009, pp. 89-94

[4] S. Hamada, M Suzuki, P. J. Maziasz, A. Hishinuma, « Microstructural evolution in austenitic stainless steels irradiated to 57 dpa in HFIR”, Journal of Nuclear Materials 179 (1991), 515-518

[5] H.A. Abderrahim, P. Baeten, D. De Bruyn, J. Heyse, P. Schuurmans,J. Wagemans, MYRRHA : a Multipurpose hYbride Research Reactor for Highend Applications, Nucl. Phys. News 20 (2010) 24-28,

[6] N. Cautaerts, R. Delville, E. Stergar, D. Schryvers, M. Verwerft, “Tailoring the Ti-C nanoprecipitate population and microstructure of titanium stabilized austenitic steels”, Journal of Nuclear Materials 507 (2018) 177-187

[7] M. Le Flem et al., “Status of the French R&D on Astrid core Materials”, Proceeding of ICAPP 2014, Charlotte, USA, April 2014

[8] P.F. Giroux and P. Olier, “Optimization and development of the manufacturing process of hexagonal wrapper tubes for ASTRID first core sub-assemblies”, Proceedings of ICAPP 2016 San Francisco, April 2016

[9] Th. Beck et al., Nuclear Engineering and Design, 315 (2017) 51-60

[10] K. Dae Whan, Journal of Nuclear Materials, vol. 420, no. 1, pp. 473–478, 2012

[11] R. Schibli R et al., “On the formation of stacking fault tetrahedra in irradiated austenitic stainless steels – A literature review”, Journal of Nuclear Materials 442 (2013) 761-767.

[12] A. Courcelle et al., “TEM Examination of a Swelling-Resistant Austenitic Steel Irradiated at High Temperature (>600°C) in the Phénix Fast Reactor”,.Proceeding of FR17, Yekaterinburg, 2017

[13] JL Seran et al., patent CEA FR 2790089-A1, 1999

[14] L. Courtin, Doctoral Thesis, Orsay University, oct. 2015

[15] A.F. Padilha et al., Journal of Nuclear Materials 105 (1982) 77-92

[16] N. Cautaerts et al., Acta Materiala 164 (2019) 90-98

[17] H.J. Beattie and W.C. Hagel. Trans. Metall. Soc. AIME, 233 (1965) 277

[18] H.J. Goldschmidt, J. Iron Steel Inst. 160 (1948) 345

[19] E. Curtet et al., “On the elementary deformation mechanisms involved in the singular behavior of 15Cr-15Ni Fuel Cladding tubes at moderate temperatures”, accepted for oral communication at TMS’2019, San Antonio, march 2019